IMPROVEMENTS IN DIELECTRIC MEASUREMENTS WITH A RESONANT CAVITY

by
Arthur J. Estin (Senior Member, IEEE)
CyberLink Corp.
1790 30th Street, Suite 300
Boulder CO 80301
and
Michael D. Janezic
National Institute of Standards and Technology
325 S. Broadway
Boulder CO 80303

Abstract: This paper describes using an automatic network analyzer to determine to very high accuracy the resonant frequency and intrinsic quality factor of a microwave resonant cavity. With this technique, measurement of complex permittivity of samples of dielectric material can be determined with low uncertainty.

Introduction

The characterization of a microwave cavity resonator requires a determination of the mode in which the cavity is operating, the resonant frequency and dimensions, the intrinsic quality factor, and various perturbations. With this characterization, the high-Q cavity resonator becomes a sensitive and accurate means of measuring the dielectric properties of material samples. The methods described in this paper make use of the high speed and built-in mismatch correction capability of an automatic network analyzer (ANA).

Circuit theory of cavity parameters

An equivalent circuit diagram of a two-port resonant microwave cavity in the vicinity of a single isolated resonance mode is shown in Figure 1. Planes a1 and a2 are arbitrary, and represent the planes of calibration of the ANA. Planes b1 and b2 are specific locations called the "planes of the detuned short circuit" at which the phase shifts corresponding to the distances d1 and d2 exactly cancel the respective self reactances X_1 and X_2 of the coupling ports at resonance. Both transmission lines connecting the ports to the ANA are assumed terminated at the ANA in their characteristic impedance Z_0.

As seen from the reference planes b1 and b2, the reflection coefficient S_{ii} for either port, as a function of frequency, is a circle whose center is on the negative real axis in the complex plane. The distance u_0 from the origin to the center is

$$(1) \quad u_{oi} = \frac{1 + \beta_n - 2r_i}{1 + \beta_i + \beta_n}$$

and the radius a of the circle is

$$a_i = \frac{\beta_i(1 - 2r_i)}{1 + \beta_i + \beta_n} \qquad (2)$$

in which the β's are the coupling coefficients and r is the port loss normalized to the characteristic impedance. The subscripts i and n refer respectively to the port being measured and the opposite port. Thus, if i=1, then n=2, and vice versa. In the limit of lossless coupling ports, the circle will pass through the point (-1,0) in the complex reflection plane. The port losses r_i are of the order of 0.001 and are neglected in the calculations.

Next, we obtain an expression for the squares of the magnitudes of the transfer scattering coefficients S_{21} and S_{12}, which because of reciprocity are identical. Solving the circuit of Figure 1 for the ratio of power transmitted to a load Z_0 on one side to the available power on the other side, we have

$$|S_{ni}|^2 = \frac{4\beta_1\beta_2}{(1 + \beta_1 + \beta_2)^2 + |\Psi - \beta_1 r_1 - \beta_2 r_2|^2} \qquad (3)$$

The quantity Ψ is a radian frequency parameter, and is given by $\delta\omega/\Delta\omega$, where $\delta\omega$ is the difference between the measurement frequency and the resonance frequency, and $\Delta\omega$ is the shift in frequency needed to move from the transmission maximum to the point either side of this maximum where the transmission has decreased by 3 dB. Eqn (3) describes a characteristic resonance curve.

Finally, we use Figure 1 to determine an expression for the loaded quality factor Q_L. The dissipated energy includes ohmic and polarization losses within the cavity and loss of stored power through the coupling ports. (Excluding the last component from the calculation would yield the uncoupled or intrinsic Q, Q_0.) Q_L is given by

$$Q_L = \frac{\omega L_{total}}{R_{total}} = \left(\frac{Q_o}{1 + \beta_1 + \beta_2}\right)\left[1 + \beta_1\left(r_1 + \frac{L_1}{M_1}\right) + \beta_2\left(r_2 + \frac{L_2}{M_2}\right)\right] \qquad (4)$$

Especially for small coupling, β<<1, the factor in square brackets is very nearly one and is ignored.

Cavity measurement techniques

Measurements of the important cavity parameters have been made for many years in either reflection or transmission mode by locating the amplitude extremum and the half-power points. Modern measurement methods using an ANA permit two significant advances over this traditional approach. First, calibration corrections built into the operating software for the ANA remove to a large extent multiple reflection and absorption errors resulting from residual component and connector mismatches and losses in the measurement system. This is particularly important when making scattering parameter measurements on a highly reflective two-port device such as a resonant cavity. Second, the capability of the ANA to rapidly make and record multiple measurements at a large number of frequencies enables measurement uncertainties to be greatly reduced with respect to both random and certain systematic errors. In addition, once a complete calibration has been carried out at a predetermined set of frequencies, measurements of all four scattering parameters can be performed in one pass.

Determination of the coupling parameters

The results of Eqns (1) and (2) suggest a very accurate method of determining the coupling parameters β_1 and β_2. If a number of reflection measurements is taken over a frequency band of at least 15 to 25 half-widths ($\Delta\omega$), then a circle in the complex reflection plane can be fitted to these reflection points for each of the Port 1 and Port 2 reflections by a linear least-squares regression process. The radii of these circles can thereby be obtained from a statistical combination of many independent measurements. These two radii determine β_1 and β_2 from the following:

$$\beta_i = \left(\frac{a_i}{1 - a_1 - a_2}\right)(1 + 2r_i) \qquad (5)$$

CH2940-5/91/0000-0573 $1.00 C 1991 IEEE

where i = 1 or 2. Again, the r's can be neglected.

Because equal frequency spacing of the data maps into an unequal point spacing, the two quadrants of the circle corresponding to the wings of the resonance curve contain many more points than the other two quadrants, which map into the region between the half-power points. Accordingly, a weighting function is used in the regression fit to equalize the importance of each of the four quadrants of the circle. In the limit of an infinite number of data points encompassing the complete frequency spectrum, exact equalization can be achieved by the weighting function,

$$w(k) = \frac{K}{\pi}\left(\frac{1}{K^2 + k^2}\right) \qquad (6)$$

in which k counts the data points, both positively and negatively, starting with the point nearest the resonance frequency as k = 0. K is the number of points required to go from the peak of the resonance to either half-power point.

Determination of Q_u

We designate the maximum power transmission at ψ=0 as $|S_{max}|^4$. Neglecting the terms $\beta_i r_i$, Eqn (3) can be rearranged as

$$\delta\omega = \Delta\omega \left[\sqrt{\frac{|S_{max}|^2}{|S_{21}|^2} - 1}\right] \qquad (7)$$

Using this expression, a plot made of $\delta\omega$ as ordinate vs. the quantity in square brackets as abscissa will appear as a line whose slope is $\Delta\omega$. We may then obtain Q_u from the ratio $\omega_0/2\Delta\omega$. With uniform frequency increments the points will be uniformly spaced. A least-squares fit of the data to a line will yield a far better value for the slope than can be obtained from only the two half-power points.

Error evaluations

Systematic measurement errors

The principal error in determining the coupling coefficients results from neglecting the effects of losses in the coupling ports, which include uncalibrated waveguide losses between the plane of calibration and the port. The effect of these losses shows up as the factor $(1-2r_i)$ in Eqn (2). In principle, r_i can therefore be determined geometrically from the parameters of the least-squares fitted circle. In practice, however, the loss error is so small as to be comparable with the measurement uncertainty.

An independent check is available on the values of the β_i's as obtained from reflection measurements. Transmission measurements are essentially independent of reflection measurements. Although they are made on the same ANA, they use different hardware combinations and separate software, and occur over a different dynamic signal range. The maximum power transmission, which occurs at ψ=0, is a function only of the coupling parameters (neglecting small errors introduced by the self impedances of the coupling ports) and can therefore be used to confirm the values obtained from the reflection measurements. With this check, an upper limit of the error in measuring the two coupling coefficients can be estimated. If the discrepancy between the measured transmission at resonance and this transmission as calculated from the coupling coefficients and is attributed equally to the two coefficients, then the worst case error in either coefficient (the coefficients being nearly equal) is given by

$$\partial\beta = \frac{\beta\,(1+2\beta)}{10\log_{10} e}\,\partial T \qquad (8)$$

where

∂T = error in the power transmission measurement, in dB,

$\partial\beta$ = error in either coupling coefficient, and

β = average of the two coupling coefficients.

Systematic errors in a Q measurement could result from any of the following causes: (1) Nearby unsuppressed modes may overlap the desired mode, thereby distorting the ideal resonance shape; (2) departures from the desired amplitude detection characteristic of the ANA over its dynamic range may distort the resonance shape; (3) limitations, instabilities, and uncertainties of the ANA measurement process may fail to correct for source, load, and feed line mismatches or otherwise produce incorrect measurements; (4) uncertainties introduced in the fitting of the straight line to the transformed data may give an erroneous slope; and (5) self impedance effects of the coupling ports may be so large that the higher order factors cannot be neglected.

The first two of these errors will cause curvature to be present in the locus of the data points used for the linear fit of Eqn (3). The presence of such curvature can be ascertained by examining a plot of the data points with the superimposed linear fit, as will be shown later in the results section, or by statistical analysis.

With respect to the third error, a detailed evaluation of the ANA as a measurement tool lies beyond the scope of this paper. Using various measurement sequences, however, we can get an indication of the repeatability of the instrument.

The fourth source of error, that of accuracy of fit of the line to the data set, is related to the preceding discussion. A regression fit of a line minimizes the effects of residual parabolic curvature by approximately equalizing the distance of the line from the extreme points in the data set. If the curvature is caused by an undesired mode which is offset in frequency from the desired mode, then this asymmetry will cause the "correct" line to differ from the "best-fit" line. The difference in slopes between these two lines leads directly to an error in Q.

Two approaches are available to reduce this error. The best way, of course, is to insure that all undesired modes in the vicinity of the desired resonance are effectively suppressed. If this is not feasible, a statistical technique can be used. The effect of an undesired mode is more pronounced in the wing of the resonance than near its center. Therefore, if the data points are weighted (using Eqn (6)) to emphasize the importance of those nearer the resonance peak, the effects of the unwanted mode are reduced. Weighting also has the desirable effect of deemphasizing the data points taken at low levels where the signal to noise ratio (S/N) is worst. This latter reason for weighting is not the same as the earlier application: There all data had equal S/N, but unequal measurement point densities, whereas here the reverse is true.

The fifth source of error can be seen in the expression in square brackets of Eqn (4). For loosely coupled cavities, r_i is less than approximately 0.001. Even if the inductance terms, which are not directly known, contribute as much as ten times this error, the resultant effect on Q_0 is only 2 parts in 10^4.

It is more difficult to find direct methods for confirming the validity of Q determinations than for the coupling coefficients. Some indirect approaches do exist, however, other than the linearity check mentioned above. Q_u is measured in both the forward and reverse directions. Although the ANA software and the calibrations for these measurements are common to the two ports, the actual measurements are made with different combinations of sources and detectors. We thus obtain two essentially independent results. One indication of the measurement uncertainty is the discrepancy between these two measurements. A second check is to examine the efficiency (the ratio of the

experimentally determined Q_0 to its theoretical maximum for the bulk metal). Expected values for a well constructed cavity should lie between 75 and 85%. Moreover, if the cavity is tunable over at least two longitudinal modes, the actual ratios for the different modes should closely agree with each other.

Interfering modes

Since a high Q_0 in the cavity improves overall sensitivity in measurements, it is desirable to select a mode which has an intrinsically high Q. This implies a large volume cavity, for the Q increases with the characteristic linear dimensions. The cavity used in these experiments operates in the circular TE_{01n} mode, n ≈ 24. It has a high Q in consequence of a large volume in which, however, somewhat over 200 other undesired modes[4] could exist. The TE_{0mn} family fortunately has the unique desirable characteristic that surface currents on the cavity walls are entirely circumferential. This permits the use of anisotropically (helically) conducting walls to suppress non-TE_{0mn} modes.[4] The sidewalls used in the NIST cavity were adapted from helically conducting TE_{01} waveguide designed as transmission line for feeds for large antenna arrays. This waveguide was not entirely successful for the cavity application, as the TE_{12n} family were not completely suppressed. Therefore, frequency/length combinations were selected in which the undesired modes are as far away as possible from the desired modes in the empty cavity.

Frequency and Dimensional Errors

The frequency at which the resonance occurs has been traditionally determined by measurement of the location of the dip (in reflection) or of the peak (in transmission). This is not exactly correct. The most important error in the determination of the frequency arises from the finite conductivity of the cavity walls. The fact that the skin depth is not zero results in decrease in the resonant frequency of the cavity. The storage of magnetic energy in the walls is greater than the corresponding electric energy by a factor of the order of 10^0 for copper at 10 GHz. A calculation shows that the resonant frequency shifts by almost exactly one half-width, $\Delta\omega$. Thus, the true value of the resonance frequency for the empty cavity can be obtained from the peak frequency and Q_0.

The effective dimensions of the cavity can be determined from frequency measurements using a minimum of two different modes, provided that the speed of free space EM propagation is corrected for moist air. If the uncertainty in length is ∂L, then the corresponding uncertainty in the resonant frequency is given by

$$\left|\frac{\partial f_o}{\Delta f}\right| = \left|\frac{\partial L}{\delta}\right| \qquad (9)$$

where

Δf = half width of the resonance,
∂f_0 = uncertainty in the resonance frequency, and
δ = skin depth.

Since the skin depth is approximately 0.8 μm (0.0008 mm), having the absolute frequency known to a half width, or 60 kHz., would set the dimensional uncertainty at the order of one μm or about 1 part in 10^9. This is consistent with differential setting and length accuracies available with the capacitative length gauge and the precision system used to drive the cavity end plate. The absolute frequency uncertainty of the ANA is about 10^{-7}, which at 10 GHz would correspond to the order of 0.02 of a half-width.

The fractional accuracy required for the speed of EM waves in air is equal to the fractional uncertainty in frequency. Thus, the index of refraction should be measured to better than ±5N where $N_\nu = (\nu - 1)\ 10^6$, ν being the index of refraction of air[3]. The uncertainty in N has the following relationship to uncertainties in temperature, total air pressure, and water vapor pressure, where the coefficients apply to typical laboratory conditions in Boulder:

$$\partial N = 1.1\,\partial T + 0.3\,\partial p + 4.1\,\partial e \qquad (10)$$

T is the temperature in Kelvins, p is the atmospheric pressure in cPa, e is the partial water vapor pressure in cPa and the partial derivative sign represents the error in each quantity. Thus, the error contributed by temperature for an uncertainty of 1N is approximately 1 K, by pressure, four cPa uncertainty, and 0.25 cPa uncertainty in water vapor pressure. Since the saturation water vapor pressure at 23°C and 840 cPa is about 23 cPa, this implies that the relative humidity must be observed to within 2%, which is far beyond the accuracy of typical hair hygrometers. A difference in temperature between the cavity water jacket and ambient laboratory temperature can cause additional temperature errors, depending upon the thoroughness and frequency with which air in the cavity is flushed out.

There is, of course, a dependence of the atmospheric parameters among themselves. Specifically, water vapor pressure is sensitive to both total air pressure and air temperature.

An additional offset in the true resonant frequency results from losses in the coupling ports, r_i, as can be seen in Eqn (9). If $r_i \approx 0.001$ and $\beta_i \leq 0.03$, then this bias is about 0.0006 which is negligible in comparison with a single step in measurement frequncy (5 kHz) for which $\psi = 0.07$.

Experimental results

NIST has designed and constructed a cavity which operates near the center of the 8 to 12 GHz frequency band. This cavity has precise length adjustment and incorporates a means of introducing dielectric samples into one end without altering the length setting. It has a capacitative micrometer to measure displacement of the end plate to a precision of 0.0001 mm. The length of the cavity is variable from about 410 to 435 mm, and it is nominally 60 mm in diameter. Although cutoff for the TE_{02n} modes is only slightly above 11 GHz., they are also discriminated against by coupling configuration.

Measurements were made of the NIST cavity at four frequency ranges, centered at 10.05, 10.34, 10.63, and 10.92 GHz. For convenience, these are designated hereafter as frequencies A, B, C, and D, respectively. The range of travel of the lower endplate permitted the cavity to be resonated in modes with longitudinal indices from 23 to 26 in various of these frequencies, and by introducing a substitute endplate with gauge block spacers, down to n = 20. Table 1 identifies the modes examined at each frequency both with and without the substitute endplate. Mode interference, which will be discussed later in detail, is indicated in qualitative degree by the code in parenthesis.

The design of the cavity was successful in suppressing most of the potentially interfering modes. A notable exception was the TE_{12n} family, which is coupled by the same iris configuration that is used to excite the desired TE_{01n} family. For reasons related to structural details of the helical waveguide used for the sidewall, which are undiclosed information of the manufacturer, this interfering family was suppressed only by a bare 15 to 20 dB. In order to examine qualitatively for the presence of these modes, uncalibrated 0.5 GHz frequency scans were taken of each of the modes examined in Table 1.

Mode Interference

Figures 2 through 5 illustrate examples of each level of interference. In each of these figures, the horizontal scale is 50 MHz per division, and the desired mode is located in the center. The vertical scale is 5 dB per division. In the upper left corner of each plot, there is a coded identification of the test configuration. The first letter is the frequency, which is also confirmed as the center frequency of the

scan at the bottom. The next two digits indicate the longitudinal mode number, and the last digit, 0 or 1, designates the endplate used. Figure 2, at frequency C and mode 24 (C24-1), is an example of no perceptible interference. Figure 3 (A21-1) shows slight interference. Figure 4 (C23-1) shows moderate interference. Finally, Figure 5 (B24-0) shows severe interference, in which the interfering mode is virtually indistinguishable from the desired mode.

Calculating the interaction of multiple modes is difficult, as the ideally orthogonal modes are actually coupled to each other through second order effects such as field distortion produced at the irises and finite conductivity of the cavity walls. Therefore, it is more effective to eliminate interfering modes than to attempt to compensate for their effects by computation.

Following the procedure described earlier, a least-squares fit of the data to a circle was performed for each case using the appropriately weighted complex reflection values. Sixty-four averaged measurements were taken every 5 kHz at 401 points across the resonance. As a verification, the maximum measured transmission was compared with that value calculated from the two coupling coefficients. In almost every case this difference was less than 0.01 dB, in one case only 0.0003 dB. Where the difference was greater than 0.01 dB, some level of mode interference was always found to be present. From Eqn (8), the uncertainty in each coupling coefficient is estimated to be less than 0.00007. As can be seen from Eqn (4), this may affect only the fourth place of Q_0. Figures 6 and 7 show plots of the circle fits achieved in two cases. Figure 6 (B23-0) represents a typical case without mode interference. (For convenience the plot is mirror reflected to the right half plane.) The dots are the actual data points, and the line is the fitted circle. Figure 7 (B24-0) is a similar plot in which severe mode interference is present. There is a slight offset of the tails of the mode from the fitted circle, but one can conclude from both of the above checks that coupling is not significantly affected by mode interference.

Determination of Q_0 and Skin Depth

A value for Q_0 was found for both the forward and reverse directions for each frequency/mode combination measured. We eliminated measurements which exhibited significant mode interference. Q_0 was obtained from the analysis of all the remaining data. Forward and reverse values were averaged for each case. This average was then divided by a calculated theoretical value and expressed as a percentage. The calculated value is based upon an optimum bulk conductivity for copper of 5.800×10^7 S/m. Values for this ratio, which we designate the "efficiency" are shown in Table 2. Those efficiencies which apply to the normal endplate "0" are encased in square brackets, and those taken with the substitute endplate "1" are unbracketed.

A consistent difference between the "1" and "0" measurements indicates that the surface conductivity of the normal endplate is approximately 15% lower than that of the substitute. There are several possible explanations of this: (1) Visible scratches on the normal endplate have resulted from possibly abrasive dielectric samples placed in the cavity. Scratches perpendicular to surface current flow will increase the effective resistance of the surface. (2) Microscopic amounts of lossy dielectric samples may have become embedded in this end plate, thus also increasing its resistivity. (3) The original surface received a gold flash of unknown thickness, and gold has a lower conductivity than copper. Moreover, there are indications that atoms migrate slowly across the gold-copper interface and form an alloy exhibiting a lower conductivity than that of either pure material[1].

Both the "0" and "1" cavity efficiencies show an unpredictable monotonic decrease with increasing frequency. We attribute this to some as yet unknown component, such as an anomalous electrical loss in a binder or insulation in the helically wound sidewall which increases more strongly with frequency than the surface resistivity of a pure metal.

Determination of cavity dimensions

Because of questionable repeatability experienced with the ANA measurements, the accuracy with which the effective diameter and the absolute length of the cavity can be determined is not clear. Our best estimate for the diameter is 60.003 mm, which is consistent with the value of 60 mm quoted by the manufacturer. Inasmuch as there is no way of maintaining an absolute reference micrometer reading, the length must be calculated at each measurement from the diameter, the resonant frequency, and the atmospheric parameters.

Detection of interfering modes

The presence of undesired modes was shown qualitatively in Figures 2 through 5. More positive identification is available in the process of calculating the Q_0 of the cavity. From Eqn (7), we expect the data to yield a line. Significant departure of the data from a line is the result of one or more effects which distort the shape of the resonance curve. The principal cause of distortion is the presence of an excited overlapping mode, whose effect is a combination of ordinary superposition and of more complicated coupling of the fields comprising the two modes. If such an interfering mode is present, the data points in Eqn (7) no longer follow a line. Thus, we can examine plots of the difference between data points and the fitted line for a sensitive empirical measure of this source of error. (Small amounts of waviness very near the resonant frequency result from imprecise location of the actual peak, and do not significantly affect the slope determination.)

Figures 8 through 11 show this difference between the fitted line and the data points for the same cases illustrated in Figures 2 through 5. The degrees of curvature in these four cases vary from no perceptible interference through severe interference. The amount of curvature which is tolerable relates directly to the error produced in the measured slope.

Measurement of Sample Dielectric Constant and Loss Tangent

When a slab of low loss dielectric is inserted into a resonant cavity, the effect is to detune the resonant frequency, because of added capacitance, and to reduce the Q, because of added dissipative absorption. The complex permittivity of the material can therefore be deduced from these measured changes. (As a matter of convenience, it is preferable to retune the cavity to its original resonant frequency by altering its length, rather than use the frequency detuning as the measure of the change.)

The necessary derivations will not be repeated here, as they have been fully developed in the literature[3]. Cook derives a solution for the complex dielectric constant of a cylindrical slab filling one end of a TE_{01n} cavity. The exact solution for the real part of the dielectric constant is transcendental, in terms of the change of the cavity parameters. It is given by

$$\frac{\tan k_g' b}{k_g' b} = -\frac{\tan (k_g L' - k_g b)}{k_g b} \qquad (11)$$

where

L' = cavity length as resonated with the sample,

b = sample length, and

k_g and k_g' are the guide wavenumbers in air and in the dielectric, respectively.

With k_g' known, the desired real part of the relative dielectric constant of the sample is

$$\epsilon_1 = \frac{k_g'^2 + \left(\frac{2\rho}{D}\right)^2}{k_g^2 + \left(\frac{2\rho}{D}\right)^2} \qquad (12)$$

where ρ is the root of the appropriate Bessel function and D is the cavity diameter.

The loss tangent is found from the uncoupled Q of the cavity with the dielectric slab inserted, after the real part of the dielectric constant is calculated. In order to separate out the effects of cavity wall losses, it is necessary to calculate the wall losses for a hypothetical configuration of the cavity containing an ideal lossless dielectric of the same size, shape, and dielectric constant as the sample under test. The parameters needed for this calculation are the skin depths of the sidewall and endwalls of the cavity, which are not necessarily equal. This is discussed in Appendix A.

From the energies stored in the dielectric and in the empty portion of the cavity, and the energies dissipated per radian as wall losses and dielectric losses, the following expression can be obtained for tan δ of the dielectric:

$$\tan\delta = \left(\frac{1}{Q_d} - \frac{1}{Q_d'}\right)F \qquad (13)$$

where

Q_d = Measured Q_0 of cavity with dielectric sample
Q_d' = Calculated Q_0 with hypothetical lossless sample.

Expressions for Q_d' and the factor F, which accounts for the fact that the dielectric only partially fills the cavity are given by Cook[5].

A sample to be measured may be machined to a diameter smaller than the cavity, either by accident or intentionally. In addition, when the undersized sample is placed on the endplate and inserted into the cavity, its location on the endplate is not necessarily centered. The error introduced by both effects can be calculated by a first order perturbation technique.

The energy change resulting from the fact that the dielectric material which no longer fills its intended volume can be related to a shift in resonant frequency, and therefore to an error in length equivalent to retuning to cavity to its original frequency:

$$\partial L = \left(\frac{\lambda_g}{\lambda}\right)^2 D\rho^2 (\epsilon_1 - 1)\left\{\frac{\zeta}{a}\left[\frac{2}{3}\left(\frac{\zeta}{a}\right)^2 + \left(\frac{\eta}{a}\right)^2\right]\right\} \qquad (14)$$

where

∂L = error in length setting of the cavity,
λ_g = guide wavelength,
a = cavity radius,
ζ = difference between cavity radius and sample radius, and
η = offset of the sample axis from cavity axis.

Results and Discussion

Preliminary measurements were made on four samples of rexolite of various thicknesses. The results are listed below:

Sample Thickness		Dielectric Constant	Loss Tangent
2.4 mm	(0.094 in)	2.536	0.00360
4.8	(0.188)	2.542	0.00075
7.2	(0.282)	2.534	0.00076
9.6	(0.376)	2.531	0.00084

Instability and lack of repeatability of the ANA caused major limitations of accuracy. A series of ten measurements of Q were rapidly made without any change in system configuration. These exhibited peak Q variations of more than five parts per thousand, even though each measurement was the average of 64 passes. Successive measurements interspersed with recalibration also show similar lack of repeatability. The exact malfunction of the ANA has not yet been identified, although coaxial cable instability is suspected.

A second difficulty relates to the presence of the undesired TE_{12n} modes in the cavity. Although the length and frequency for the measurement of the empty cavity can be selected to avoid mode interference, the insertion of the sample can unpredictably shift one of these undesired modes into a condition of overlap, with resultant loss of accuracy. This emphasizes the need for good mode purity in the basic cavity design.

Appendix A. Wall losses

In order to measure the loss tangent of a dielectric sample, the effect of wall losses must be separated from that of the dielectric losses. To relate the wall losses as measured in an empty cavity to those experienced when the lossy dielectric sample is inserted into the cavity, the wall loss parameter called "skin depth," $\delta = (2/\omega\mu\sigma)^{1/2}$, must be determined from the measurement of Q_0 of the empty cavity.

Because the high mode cavity used for this measurement achieves suppression of unwanted modes by using a composite sidewall structure, it is desirable to measure the skin depth of the endwalls separately from that of the sidewall. The expression

$$\frac{1}{Q_0} = \left(\frac{2\rho^2\lambda^2}{\pi^2 D^3}\right)\delta_s + \left(\frac{\lambda^2}{2(\Delta L)^2 L}\right)\delta_e \qquad (15)$$

where

ΔL = Change in length of the cavity for a unit longitudinal mode index change,
λ = Free space wavelength, and
L = Length of the cavity,

relates Q_0 for the empty cavity to the skin depths of the sidewall, δ_s, and the endwalls, δ_e, in terms of the cavity dimensions, mode parameters, and free space wavelength:.

If measurements of Q_0 were made at constant frequency and varying longitudinal mode index, we could plot $1/Q_0$ vs. 1/L and determine the values of δ_s and δ_e from the y-intercept and slope, respectively, of the resulting best-fitted line. However, this would require unattainably large travel of the end-plate to extend n far enough to achieve good accuracy with the extrapolation. Therefore, if sufficiently good accuracy can be obtained in the measurements of Q_0, these quantities can be uniquely determined by making two measurements, for example, at n = 24 and n = 25, and solving simultaneously the resultant forms of Eqn (15). If the accuracy of Q measurement is not sufficient to permit using the small difference of the reciprocal Q's, then a single composite value of the skin depth can be obtained by assuming $\delta_s = \delta_e$ and averaging the results of the n = 24 and n = 25 measurements. The error resulting depends upon the magnitude of the actual difference between the skin depths.

References

[1.] F. K. Richtmyer and E. H. Kennard, Introduction to Modern Physics. New York: McGraw-Hill, 1942, p. 189.

[2.] A. J. Estin, "High mode tunable cavity for microwave-gas interactions," vol 33, pp. 369-371, April 1962.

[3.] B. R. Bean and E. J. Dutton, Radio Meteorology. New York: Dover Publications, Inc., 1968, p. 7.

[4.] W. Jost, Diffusion in Solids, Liquids,, and Gases. New York: Academic Press, 1952, p 121.

[5.] R. J. Cook, "Microwave cavity methods," in High Frequency Dielectric Measurement Conference Proceedings, J. Chamberlain and G. W. Chantry, Eds. Guilford, U.K.: IPC Science and Technology Press, 1973, pp 12-27. (Cook summarizes and includes references to many earlier works contributing to these results.)

[6.] R. J. Cook, op cit.

Mode	Freq. A	Freq. B	Freq. C	Freq. D
20			1*	
21	1?		1*	
22	0! 1!	1*	1*	
23	0*	0* 1*	1!	
24		0!!	0* 1*	1*
25			0*	0!! 1!!
26				0*

Table 1. Modes examined in NIST cavity.

KEY to Table 1

0 = Normal endplate 1 = Substitute endplate

Presence of Interfering TE_{12n} Modes:

* = Imperceptible; more than 50 MHz distant.
? = Slight; 25-50 MHz distant.
! = Moderate; closer than 25 MHz; distinguishable
!! = Severe; closer than 25 MHz and indistinguishable

Mode	Freq. A	Freq. B	Freq. C	Freq. D
20			78.46	
21	80.49*		78.27	
22		79.97	78.70	
23	[78.13]	79.42 [76.77]		
24			78.84 [75.68]	76.86
25			[75.50]	
26				[74.93]
Avg	80.49 [78.13]	79.70 [76.77]	78.57 [75.59]	76.86 [74.93]

Table 2. Mode efficiencies.

Notes: (1) Values in square brackets are with normal endplate, "0"; unbracketed values are with the substitute endplate, "1".

(2) Value marked with an asterisk has a mode interference, "slight" as defined in Table 1. All other values have no perceptible interference.

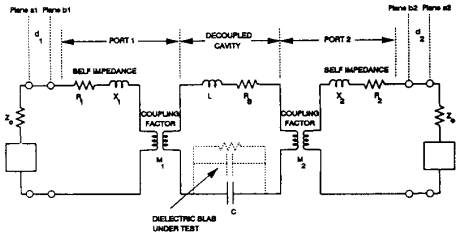

Figure 1 EQUIVALENT CIRCUIT OF A TRANSMISSION (2-PORT) CAVITY

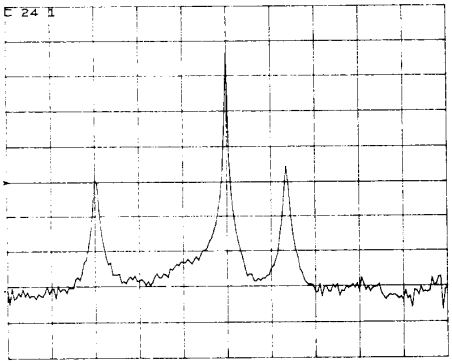

Figure 2 NO PERCEPTIBLE MODE INTERFERENCE

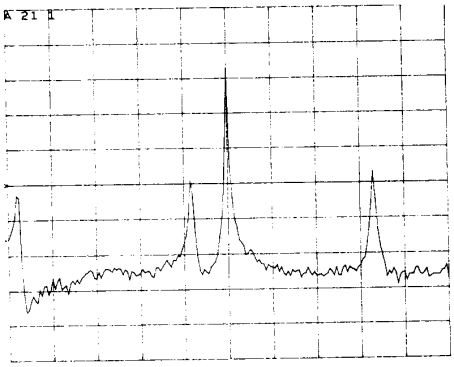

Figure 3 SLIGHT MODE INTERFERENCE

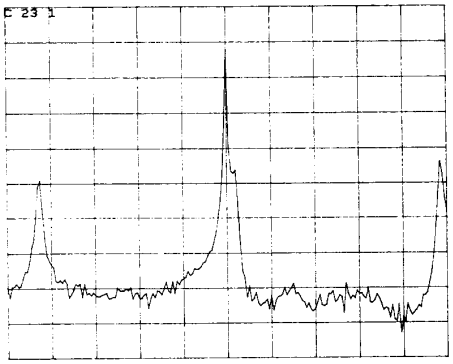

Figure 4 MODERATE MODE INTERFERENCE

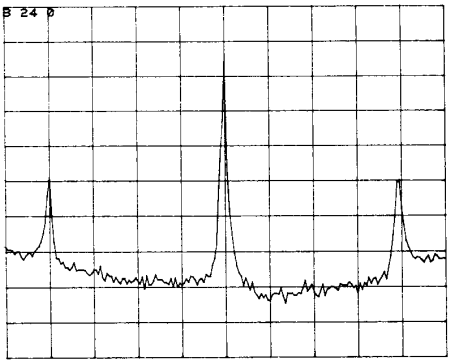

Figure 5 SEVERE MODE INTERFERENCE

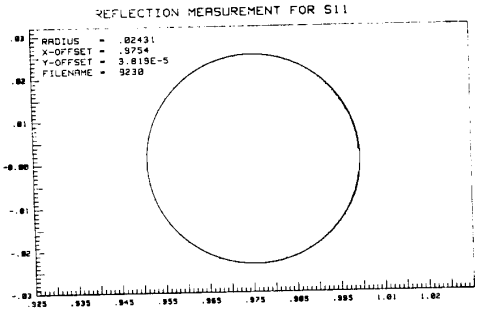

Figure 6 REFLECTION WITH NO INTERFERENCE

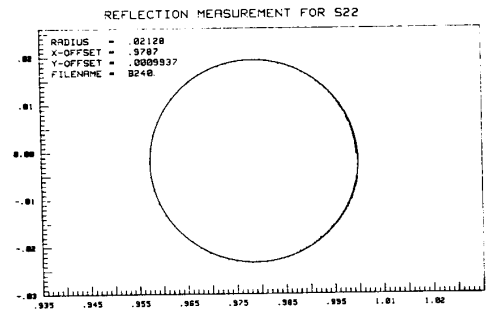

Figure 7 REFLECTION WITH SEVERE INTERFERENCE

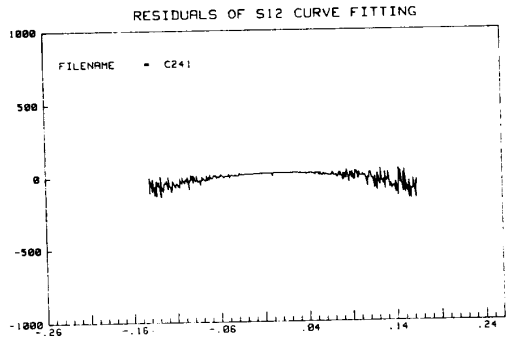

Figure 8 DEVIATION FROM STRAIGHT LINE: NO INTERFERENCE

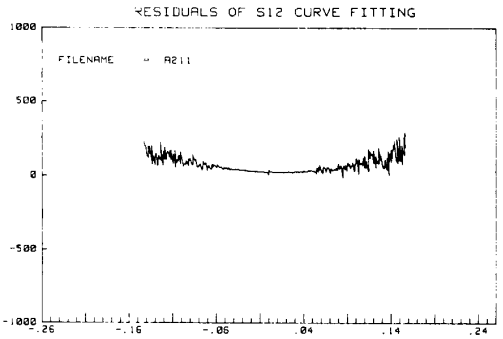

Figure 9 DEVIATION FROM STRAIGHT LINE: SLIGHT INTERFERENCE

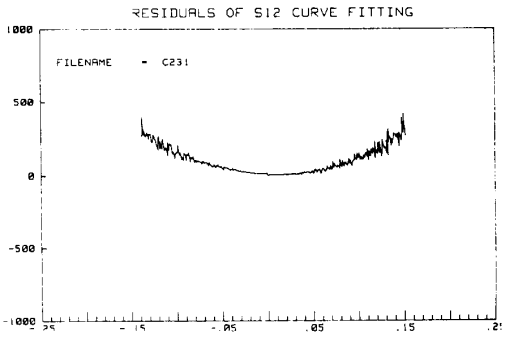

Figure 10 DEVIATION FROM STRAIGHT LINE: MODERATE INTERFERENCE

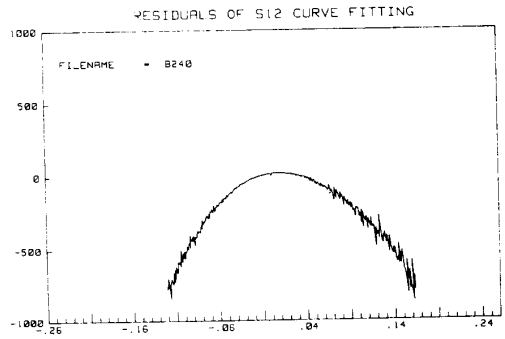

Figure 11 DEVIATION FROM STRAIGHT LINE: SEVERE INTERFERENCE